ELSEVIER

Polymer 43 (2002) 3239–3246

polymer

www.elsevier.com/locate/polymer

Spatial effects in the photodegradation of poly(acrylonitrile–butadiene–styrene): a study by ATR-FTIR

Jayesh G. Bokria, Shulamith Schlick*

Department of Chemistry, University of Detroit Mercy, Detroit, MI 48219-0900, USA

Received 1 November 2001; received in revised form 31 January 2002; accepted 4 February 2002

Abstract

Spatial effects in the degradation of poly(acrylonitrile–butadiene–styrene) (ABS) exposed to UVB radiation ($\lambda = 290$–330 nm) and oxygen in a weathering chamber at 318 K were studied by attenuated total reflectance Fourier transform infrared spectroscopy (ATR-FTIR). The polymer contained 2 wt% Tinuvin 770, a hindered amine stabilizer (HAS). ABS samples of thickness 4 mm were irradiated, microtomed, and sections of thickness 50 and 150 μm were studied as a function of treatment time. ATR-FTIR profiling indicated that the degradation was spatially heterogeneous: significant amounts of photoproducts were detected only in the directly irradiated layer of depth ≈ 50 μm. In this layer, major damage was reflected in the appearance of the hydroxyl (3600–3200 cm^{-1}) and the carbonyl (1800–1600 cm^{-1}) peaks, and in the disappearance of the 967 cm^{-1} peak from 1,4 butadiene units (1,4 PB). The hydroxyl and carbonyl peaks were also detected in the second layer of thickness ≈ 50 μm. Slight changes in the intensity of peaks in the above three spectral regions, compared to a nonirradiated reference sample, were also detected on the nonexposed sample side, and assigned to thermal degradation. For irradiation times up to ≈ 2000 h, the spectra indicated damage of the butadiene structure, and no changes in the styrene–acrylonitrile (SAN) matrix. The present study confirmed major conclusions deduced from 1D and 2D nondestructive electron spin resonance imaging (ESRI) experiments performed on the same samples in our laboratory, and provided additional information on the spatial distribution of stable degradation products.

Keywords: Poly(acrylonitrile–butadiene–styrene); Photo and thermal degradation; Diffusion-limited oxidation

1. Introduction and background

Poly(acrylonitrile–butadiene–styrene) (ABS) polymers rank second only to nylon in their importance as engineering polymers in the US, due to their attractive mechanical properties and convenient processing conditions [1–3]. The polymers consist of an elastomeric component, usually polybutadiene (PB), dispersed in a copolymer of styrene (S) and acrylonitrile (AN); PB and the thermoplastic component (SAN) become compatible due to grafting of SAN on the elastomer chains. The resulting complex polymeric materials are phase-separated into B-rich and SAN-rich domains [4–6], but the specific morphology depends on the preparation method [3]. In emulsion polymerization, a PB latex is further polymerized at ambient temperature in the presence of S and AN, leading to a dispersion of PB-*g*-SAN in a continuous SAN phase; the size of the rubber particles is in the range 0.1–1 μm. In mass polymerization, S and AN monomers are grafted to linear PB chains at elevated temperatures, ≈373 K, in the absence of solvent; this process results in larger rubber particles, typically 0.5–5 μm, that also contain occluded SAN. The properties of ABS polymers can be modified by variation of the grafting conditions and monomer ratio, to produce a polymer suitable for specific applications [4–6].

ABS polymers are susceptible to oxidative degradation when exposed to heat, mechanical stress and ionizing or UV irradiation in the presence of oxygen, due to the formation of reactive intermediates such as free radicals (for instance, R· and ROO·) and hydroperoxides, ROOH. Modification of the chemical structure of polymers due to degradation leads to changes in the molecular mass, degree of crystallinity, and mechanical properties [7–9]. A variety of additives (light and thermal stabilizers, antioxidants) are usually included in ABS formulations in order to protect the structure and extend polymer lifetime [10]. Numerous studies have addressed the challenge of understanding the

* Corresponding author. Tel.: +1-313-993-1012; fax: +1-313-993-1144.
E-mail address: schlicks@udmercy.edu (S. Schlick).

0032-3861/02/$ - see front matter
PII: S0032-3861(02)00152-0

(a) Repeat Units in ABS Polymer

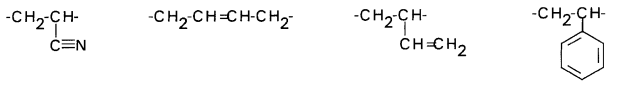

1,4-trans- and cis- *1,2 vinyl-*

Acrylonitrile (AN) *Butadiene (B)* *Styrene (S)*

(b) Hindered Amine Stabilizer (HAS): Tinuvin 770

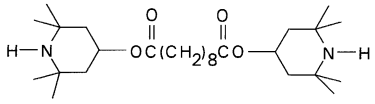

Chart 1. (a) Repeat units in ABS polymer; (b) hindered amine stabilizer (HAS): Tinuvin 770.

complex degradation kinetics and mechanism, and the effectiveness of the additives [6–11].

Fourier transform infrared (FTIR) spectroscopy is an important tool for investigating polymer degradation, because of its ability to detect stable degradation products. In the case of photo-oxidation of polystyrene [12] and poly(α-methylstyrene) [13], for example, absorptions in the carbonyl and hydroxyl regions as a function of irradiation time have led to the identification of a number of degradation products and to a proposed reaction scheme. In many cases the mechanism and extent of degradation, and the corresponding degradation products, depend on the irradiation wavelength. In the case of polystyrene, similar photoproducts but in different concentrations have been detected for irradiation with short and long wavelength, $\lambda = 253.7$ and ≥ 300 nm, respectively [12].

FTIR spectroscopy has also been used to follow the photodegradation of ABS polymers in the presence of oxygen [14–16]. Jouan and Gardette have investigated exposure to radiation $\lambda > 300$ nm of ABS films with thickness in the range 42–211 μm, as well as 'packed-multilayers', samples composed of several films separated by a layer of cardboard that allowed oxygen penetration [14,15]. The results have indicated that the extent of degradation depends on the film thickness, and that directly exposed layers show more damage compared to the interior layers. As expected, the butadiene component was found to be the most susceptible to degradation [14]. UV-absorbing photoproducts have been assigned to the degradation of polystyrene, initiated by diffusion of radicals formed in the butadiene phase into the SAN phase [15].

Photoacoustic (PA) FTIR spectroscopy has been used to follow nondestructively chemical changes in ABS polymers at depths in the range 5–16 μm from the irradiated side. The spectra were measured after exposure of the samples in the interior of cars, Florida exposure, and Xe-arc irradiation in a weathering chamber [16]. This study has indicated that the

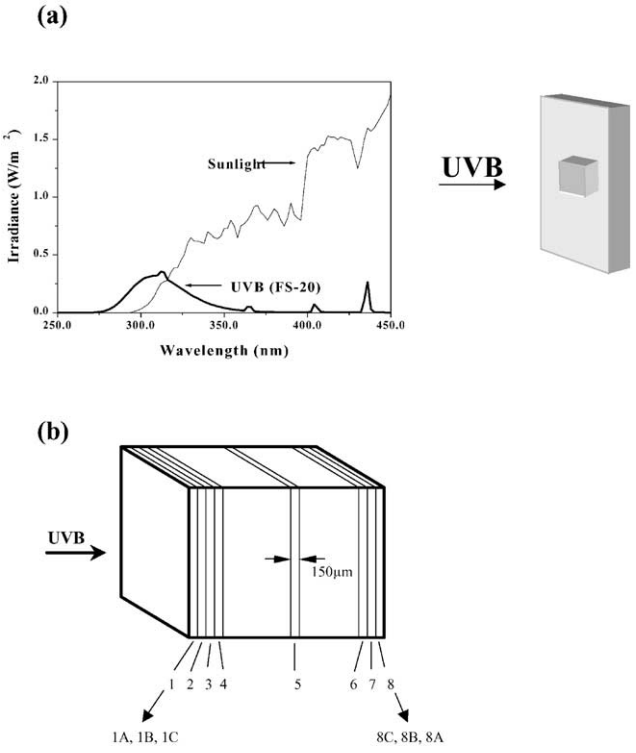

Fig. 1. (a) Spectral range of the UVB source, compared to sunlight, and sample configuration. (b) Location of sections 1–8 (thickness 150 μm), and slices 1A–C, 8A–C (thickness 50 μm).

B and AN components are degraded more extensively than the S component.

Infrared microspectroscopy has been used for profiling the thermal oxidative products in nitrile rubber; the spatially heterogeneous degradation has been explained by diffusion-limited oxidation (DLO) [17]. The IR intensity of the AN component was not affected by thermal treatment up to 413 K.

Published degradation studies on ABS have suggested that structural changes depend on the irradiation wavelength. To the best of our knowledge, the effect of UVB radiation (290–330 nm) on ABS polymers has not been investigated. Moreover, the IR work on ABS degradation has been performed on films or 'pressed-films' [14,15], and may not reflect DLO processes that occur in ABS polymers used in real applications.

We present an FTIR study of ABS exposed to UVB radiation and oxygen in a weathering chamber at 318 K. The polymer contained the HAS known as Tinuvin 770. Chart 1 shows the repeat units in ABS and the chemical structure of the stabilizer. The objectives of this study were to extract spatial details on the degradation process, and to complement the electron spin resonance imaging (ESRI) studies performed on the same samples in our laboratory [18–20]. An important conclusion of the imaging studies was the detection of HAS-derived nitroxide radicals mostly on the irradiated side of the sample for UVB irradiation [20], and on both sample extremities for Xe-arc

irradiation [18,19]. In both cases, however, the degradation was confined to the butadiene-rich domains. Some of the conclusions from the present study support the interpretation of the ESRI results for ABS degradation by UVB light.

In this study, we used FTIR in its attenuated total reflectance (ATR) mode. Quantitative application of the ATR method requires the use of mathematical algorithms to convert the ATR spectra to the corresponding transmission spectra. For this, the optical constants of the sample must be known and the use of polarized IR radiation is essential [21,22]. Further, the contact between the ATR crystal and the sample needs to be perfect and reproducible from sample to sample. As seen later, reproducible contact was achieved by preparing the polymer film directly from solution on the ATR crystal. Comparison of spectra was performed by correcting for the penetration depth, d_p, with change in wavelength. In this way the need for polarized radiation and extensive use of mathematical algorithms were avoided, and ATR-FTIR of ABS samples developed into a reliable method for semiquantitative depth profiling of the photo-oxidative degradation products. Some results have been recently reported [23].

2. Experimental section

2.1. Sample preparation

Experiments were performed on ABS (Magnum 342 EZ from Dow Chemical Company, 10% B by weight) doped with 2 wt% bis(2,2,6,6-tetramethyl-4-piperidinyl) sebacate, Tinuvin 770, from Ciba Specialty Chemicals (Chart 1). The polymer and the HAS were blended, shredded, and shaped into 10 cm × 10 cm × 0.4 cm plaques in an injection molding machine at 483 K. Additional details have been reported [18–20].

Accelerated degradation experiments were performed by exposing the ABS plaques to UVB irradiation in a UV-2 Atlas Weatherometer equipped with four fluorescent lamps (FS-20) as source for the 290–330 nm range. The temperature in the irradiation chamber was 318 K. All plaques were irradiated continuously, with one side exposed to radiation, and the other (backside) covered with aluminum foil, to avoid exposure to scattered light. Fig. 1a shows the range of the UVB source compared to sunlight, and the sample configuration during irradiation. After exposure times of 72, 213, 471, 810 and 2024 h, the plaques were removed from the irradiation chamber, and two blocks of approximately 6 mm × 6 mm × 4 mm were cut from the plaques. One of these blocks was glued to a wooden dowel with superglue, with the backside in contact with the dowel and the front side exposed; the other block was similarly glued, but with the backside exposed. The dowels were used to hold the sample during microtoming. As a result of irradiation, the polymer had become brittle and hard. Microtoming the first slices from the exposed side of samples after long exposure times was difficult, and often only fragments of slices were collected in a depth of ≈100 μm. Deeper into the sample and away from the irradiated side, the sample became progressively softer and behaved as the native polymer at a depth of ≈200 μm.

Slices of thickness 50 μm were obtained by microtoming at room temperature, using a Spencer-820 rotatory microtome equipped with a stainless steel knife. In the first set of experiments, three serial slices were combined into one specimen; thus analysis was performed on 150 μm depth sections. The location of sections 1–8 in the sample is shown in Fig. 1b. In the second stage, each 50 μm slice for sections 1 and 8 was analyzed separately; the notation of these samples is 1A, 1B, 1C from the exposed side, and 8A, 8B, 8C from the unexposed side (Fig. 1b). Each sample was dissolved in 3 ml chloroform (Mallinckrodt, spectroscopic grade) by stirring for ≈2 h to ensure complete dissolution of the polymer.

2.2. ATR-FTIR spectroscopy

Spectra were acquired using a Perkin Elmer FTIR-2000 spectrometer equipped with a Mid IR (MIR) globar source and a triglycine sulfate (TGS) detector. ATR spectra were obtained with the horizontal attenuated total reflectance (HATR) accessory. The internal reflecting element (IRE) was a ZnSe crystal set at an incidence angle of 45°.

For ATR-FTIR analysis, the polymer solution in chloroform was spread on the ATR crystal and the polymer film was obtained directly on the crystal by solvent evaporation. The removal of the solvent was achieved during ≈15 min; in some samples weak solvent peaks were identified at 3020, 1215, 758, and 670 cm^{-1}, but the peaks did not interfere with the spectral analysis. ATR-FTIR spectra were collected in the range 4000–650 cm^{-1} at 1 cm^{-1} intervals, with eight scans and a resolution of 4 cm^{-1}.

ATR-FTIR is a surface technique in which the sample and the IRE are in intimate contact. The IRE has a refractive index higher than the sample; at contact, total internal reflectance occurs and an evanescent wave penetrates in the sample to a depth called depth of penetration, d_p. As shown in Eq. (1), d_p can be calculated for each wavelength if the optical constants of the polymer sample and the IRE (ZnSe) are known [21].

$$d_p = \frac{\lambda}{2\pi n_1 \left(\sin^2 \theta - n_{21}^2\right)^{1/2}} \quad (1)$$

In Eq. (1), λ is the wavelength of the IR radiation in air, θ is the angle of incidence, n_1 is the refractive index of the IRE, and n_{21} is the ratio of the refractive index of the sample to that of the IRE. The longer wavelengths penetrate deeper into the sample, and lead to a more intense absorbance. For quantitative ATR data, the thickness of the film in contact with the IRE must be greater than the calculated depth of penetration at the longest wavelength of interest. A typical

polymer has a refractive index in the range 1.20–1.60. ZnSe has a refractive index of 2.4, and $\theta = 45°$. Using these values, d_p for 650 cm^{-1}, the longest wavelength in our experiments, is in the range 2–4.5 μm. The method of sample preparation that was adopted leads to a polymer film of thickness ≈15 μm for the 50 μm thick slices, well above the penetration depth, even for the longest wavelength.

The ATR-FTIR spectra acquired were first corrected for background, based on the signal recorded for the same ATR crystal, but without the polymer film. The ATR crystal was cleaned using laboratory grade acetone; the background spectrum was checked for the characteristic acetone and ABS peaks to ensure proper removal of the polymer and cleaning solvent before the next sample was measured. Next, the spectra were corrected for ATR using a zero contact factor, which is appropriate, since the film was solvent-cast directly on the IRE. The ATR-corrected spectra were baseline corrected to compensate for fluctuations in instrument background and absorbance levels, and their intensities were normalized to the intensity of the C≡N stretch from AN at 2238 cm^{-1}, which was assumed to remain constant during degradation. This assumption is based on conclusions from the study of ABS degradation by UV irradiation with $\lambda > 300$ nm [14,15] and the thermal degradation of nitrile rubber [17]. The reproducibility of this technique was checked with nonirradiated ABS samples, each sample consisting of a newly microtomed 150 μm section. After background, ATR and baseline corrections, and normalization based on the nitrile peak, all peak positions and corresponding relative intensities were essentially the same.

3. Results and discussion

3.1. Reference spectra and peak assignment

The ATR-FTIR spectra of native ABS (without HAS) and of the corresponding homopolymers were recorded as reference. Fig. 2 presents the ATR-FTIR spectrum for nontreated ABS containing 2 wt% Tinuvin 770. The aromatic and aliphatic C–H stretches are clearly seen in the range 3200–3000 cm^{-1} and 3000–2800 cm^{-1}, respectively. The intense and well-defined C≡N stretch from AN is seen at 2238 cm^{-1}, and the ring modes of S appear at 1602 and 1494 cm^{-1}. The scissoring mode of the CH_2 groups is at 1453 cm^{-1}, and the intense ring bends are visible at 753 and 699 cm^{-1}. The C–H deformation for hydrogen atoms attached to alkenic carbons in 1,4 PB is seen at 967 cm^{-1} and in 1,2 PB at 911 cm^{-1}. The peaks taken as reference for the AN and S components appear at 2238 and 1602 cm^{-1}, respectively; peaks at 967 and 911 cm^{-1} were taken as representative of the B component. These peaks lie in spectrally clear windows, free of interference from other peaks in the spectrum, as clearly seen in Fig. 2.

The peaks at 3301 and 1728 cm^{-1} are not consistent with the components of ABS or with the spectra of the individual homopolymers. The peak at 1728 cm^{-1} is assigned to the carbonyl in the ester group of Tinuvin 770. In the IR spectrum of Tinuvin 770 dissolved in chloroform this peak appears at 1722 cm^{-1}. The red shift compared to ABS can be explained, as an ATR spectrum was acquired for the polymer containing HAS, and a transmission spectrum for the HAS solution. To confirm this assignment and rule out artifacts due to the ATR technique, ABS samples containing 1 and 2 wt% HAS were prepared in the same way as described in Section 2, microtomed, and measured by ATR-FTIR. Fig. 3 depicts changes in the carbonyl region of the spectrum of ABS containing 0, 1, and 2% HAS. The absence of the 1728 cm^{-1} peak in ABS without HAS, and its higher intensity in the sample containing 2% HAS compared to 1% HAS indicated that the peak is from the stabilizer. This simple experiment served the double purpose of confirming the peak assignment, and comparing transmission and ATR-FTIR spectra.

The 3301 cm^{-1} peak is assigned to the H-bonded N–H stretch from a noncyclic N-monosubstituted amide in its *trans* form; this peak may be enhanced via Fermi resonance with the overtone from the peak at ≈1550 cm^{-1}. The latter peak is characteristic for noncyclic N-monosubstituted amides, and arises from both C–N and C–N–H in-plane bend in the stretch–bend mode (sometimes called Amide II) [24,25]. The C=O stretch of the amide is an intense band in the range of 1680–1630 cm^{-1}. The three peaks related to this chemical moiety are seen in the ABS spectrum at 3301, 1637, and 1552 cm^{-1}, as indicated in Fig. 2. These peaks, which are very intense in a pure amide, are weak in the spectra of the ABS samples, implying a small amount of the N-monosubstituted amide. Therefore the peak at 3301 cm^{-1} is assigned to an amide additive in the original polymer supplied by The Dow Chemical Company, and may arise from a small amount of Nylon 6 added to ABS as a toughening and antistatic additive [26,27].

3.2. Depth profiling of degradation products

Degradation produces oxygen-containing groups such as esters, hydroxyls, acids, and carbonyls. Chemical processes can be followed by observing the appearance of new peaks in the hydroxyl (3600–3200 cm^{-1}) and carbonyl (1800–1600 cm^{-1}) regions, and changes in the reference signals for the S, AN, and B components in ABS.

ATR-FTIR spectra from sections 1, 5, and 8 (depicted in Fig. 1b) in ABS after exposure to UVB radiation for 2024 h are shown in Fig. 4. The hydroxyl, carbonyl, and butadiene regions are expanded in insets (a)–(c). Increased absorptions in the hydroxyl and carbonyl regions on the irradiated side are clearly seen, as well as a general increase of the baseline in the fingerprint region. The ester groups generated during degradation appear in the range 1300–

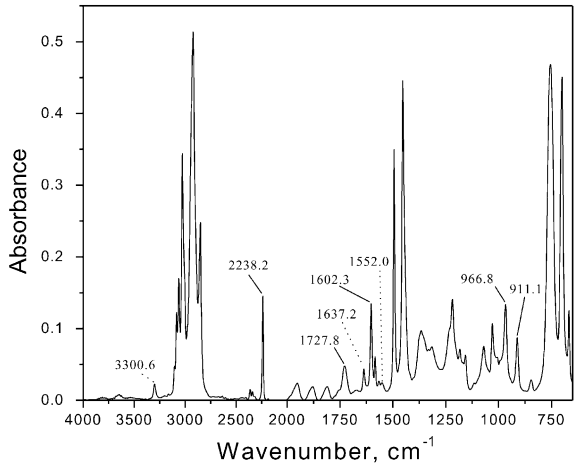

Fig. 2. ATR-FTIR spectrum of nonirradiated ABS containing 2% HAS. The peak assigned to the N-monosubstituted amide is shown at 3300.6 cm^{-1}.

1000 cm^{-1} and can be seen as a general underlying increase, but the peak positions are not clearly visible.

The hydroxyl peak appears as a broad signal with maximum at ≈3450 cm^{-1}, typical of an OH stretch. The tail of this band extends beyond 3000 cm^{-1}, suggesting the presence of OH groups from carboxylic acids. On the irradiated side, the carbonyl peak is broad, with several shoulders. On the nonirradiated side, section 8, a distinct shoulder at ≈1755 cm^{-1} is observed, which is absent in the midsection. The various types of carbonyls formed during treatment (esters, acids, ketones, aldehydes, etc.) are responsible for the shoulders and peak width. In the butadiene region, inset (c), a major decrease of the 967 cm^{-1} peak in section 1 is clearly seen, and only a slight decrease in section 8. The corresponding changes of the 911 cm^{-1} peak are less pronounced.

Higher resolution of the degradation profiling was obtained from the study of 50 μm slices; the results for samples irradiated during 810 h are presented in Fig. 5 for the three slices on the irradiated side (1A, 1B, 1C), and in

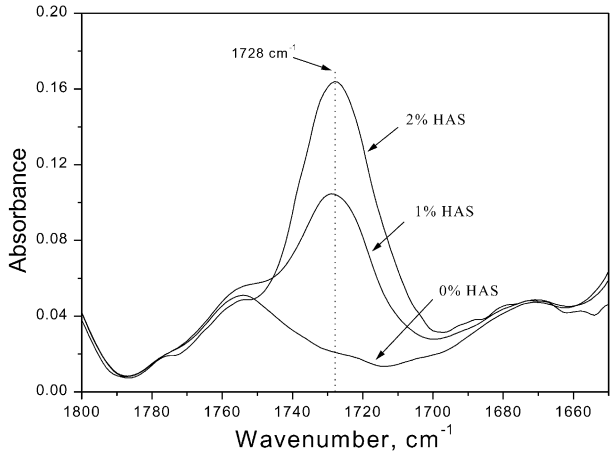

Fig. 3. The carbonyl region in the nonirradiated ABS containing 0, 1 and 2% HAS. The peak heights were normalized to the AN peak at 2238 cm^{-1}.

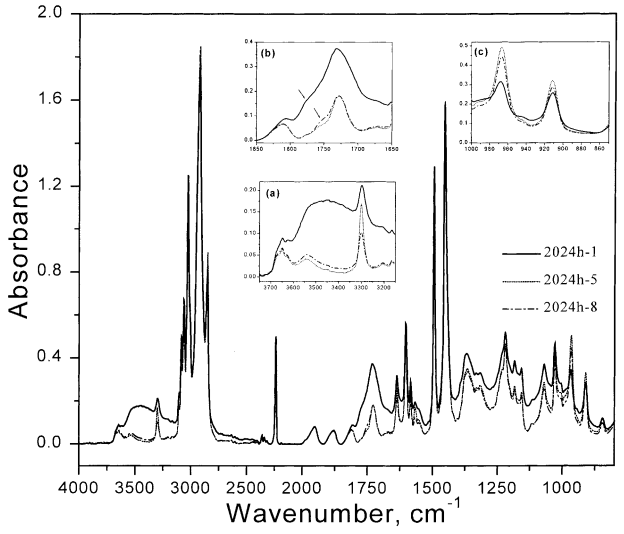

Fig. 4. ATR-FTIR spectra of sections 1, 5, and 8 (thickness 150 μm) for ABS containing 2% HAS, and UVB-irradiated during 2024 h. The insets present: a, hydroxyl region; b, carbonyl region; c, butadiene region. In inset b arrows point to shoulders from carbonyl groups formed during irradiation.

Fig. 6 for the three slices on the nonirradiated side (8A, 8B, 8C). The hydroxyl, carbonyl, and butadiene regions are expanded in insets (a)–(c) of Figs. 5 and 6. Spectra of 50 μm slices from samples irradiated during 2024 h were qualitatively similar to those presented in Figs. 5 and 6.

Several important conclusions can be deduced from Figs. 4–6.

First, in terms of hydroxyl and carbonyl peaks, the spectra presented in Fig. 4 indicate that the degradation products appear in a 150 μm-thick section on the irradiated side only, and only minor differences are detected between the midsection (section 5) and the backside (section 8). This is clearly seen in Fig. 4 for the longest treatment time, but is also true at shorter irradiation times, and can be explained by the absence of UV penetration beyond 150 μm. In terms of the butadiene peaks, spectra shown in Fig. 4 indicate that the middle section of the sample is most stable. The intensities of the 911 and 967 cm^{-1} peaks are in the order section 5 > section 8 > section 1. As we deduced that the UV penetration is not beyond 150 μm, the decrease in the butadiene peak intensity in section 8 must be due to other effects. We propose that thermal degradation is responsible, as the UV irradiation was performed in the weathering chamber above ambient temperature (318 K). This conclusion is in agreement with the ESRI study of the same samples, which has indicated the consumption of nitroxide radicals (which act as radical 'scavengers') located in the butadiene-rich domains on the back of the sample [20]. As seen in Fig. 4, inset (c), the decrease of the peak at 967 cm^{-1} on the backside compared to the midsection is rather small, ≈10%, and the major decrease is on the irradiated side, ≈40%; therefore the degradation of the B component in ABS due to thermal effects is less pronounced than that

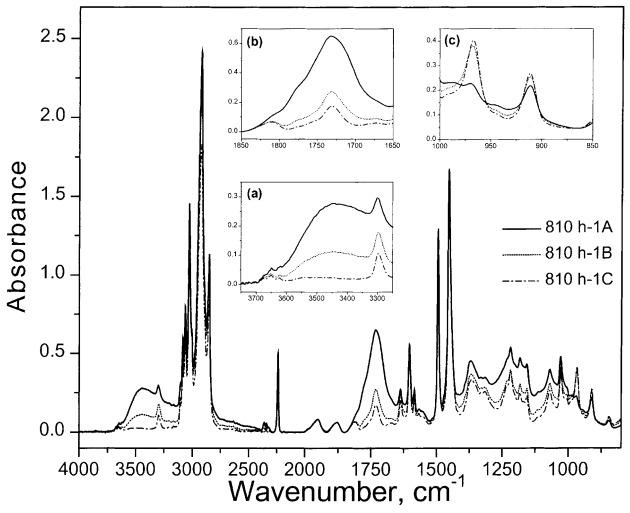

Fig. 5. ATR-FTIR spectra of sections 1A, 1B, and 1C (thickness 50 μm) for ABS containing 2% HAS, and UVB-irradiated during 810 h. Insets present: a, hydroxyl region; b, carbonyl region; c, butadiene region.

due to UVB irradiation. The decrease in the intensity of the 911 cm^{-1} peak is less pronounced than for the peak at 967 cm^{-1}, but qualitatively the same trend was observed: minimal decrease in the middle section and maximum decrease on the irradiated side.

Second, spectra shown in Fig. 5 show that the major degradation products are seen in the layer of thickness 50 μm on the irradiated side. In the hydroxyl region, however, data shown in inset a of Fig. 5 testify to the presence of a significant absorption in the *second* 50 μm layer also. In the carboxyl and butadiene regions, however, there are only minor differences in the intensities seen in the second and third 50 μm layers, as clearly seen in insets (b) and (c) of Fig. 5.

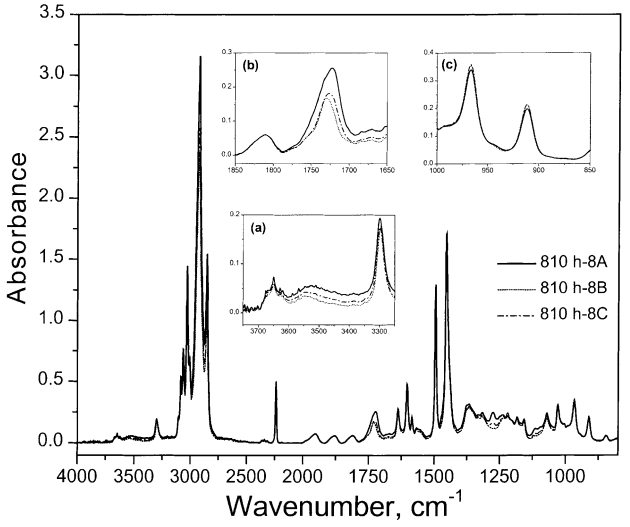

Fig. 6. ATR-FTIR spectra of sections 8A, 8B, and 8C (thickness 50 μm) for ABS containing 2% HAS, and UVB-irradiated during 810 h. Insets present: a, hydroxyl region; b, carbonyl region; c, butadiene region.

The differences on the nonirradiated side in the three spectral regions, Fig. 6, are less pronounced. This effect can be clearly understood, as for thermal degradation at a relatively low temperature, 318 K, the oxygen penetrates deeper into the sample and DLO effects are not pronounced.

Third, data in inset (c) of Fig. 5 indicate that the signal from 1,4 PB decreases significantly during photodegradation, while the signal from 1,2 PB is much less affected.

Taken together, the main conclusion derived from Figs. 4–6 is that UV-induced degradation is seen on the irradiated layer, and thermal degradation of the butadiene component is detected also on the backside. The IR spectra also indicate that the midsection is protected from degradation and shows no, or negligible, degradation effects.

The results presented above depend on the normalization procedure, based on the 2238 cm^{-1} from AN. We note that after normalizating spectra from different sections, the peaks associated with the aromatic ring in the styrene component of ABS were essentially the same, after baseline correction. Barring an unlikely coincidence, such results indicate that both the S and the AN components in ABS are not affected by UVB irradiation.

3.3. Intensity of photoproducts as a function of irradiation time

The spectral changes on section 1 (150 μm thick) as a function of irradiation time were studied in detail. The peak at 1602 cm^{-1}, chosen to represent the styrene component, remained unaltered. No change was observed in the 3200–3000 cm^{-1} region of the aromatic C–H stretch, providing further evidence that the aromatic component of the polymer was not affected by UVB irradiation.

The spectra change significantly with irradiation time in the hydroxyl, carbonyl, and butadiene regions, as shown in Fig. 7. The increase in the hydroxyl region is considerable even in the early stages of the irradiation process ($t = 72$ and 213 h), and more gradual for longer exposures. The increase in the carbonyl band, however, is minimal after $t = 72$ h and the big jump in intensity is detected after 213 h of irradiation. This result is reasonable, as peroxides are expected to appear early in the degradation process and to initiate the degradation chain.

The time dependence of the hydroxyl absorption with irradiation time for the first section, calculated by integrating the spectral region 3606–3234 cm^{-1}, is presented in Fig. 8. The time variations of the carbonyl and butadiene absorptions were also calculated, but their accuracy is limited, because only the heights can be considered; these heights are not considered representative of the intensity of broad absorptions that contain numerous shoulders. Qualitatively, the intensity of the carbonyl peak lags behind that of the hydroxyl peak, and reaches a plateau after ≈600 h of irradiation. The butadiene peak at 967 cm^{-1} decreases significantly during ≈ 300 h of irradiation, and the decrease is considerably slower for longer treatment

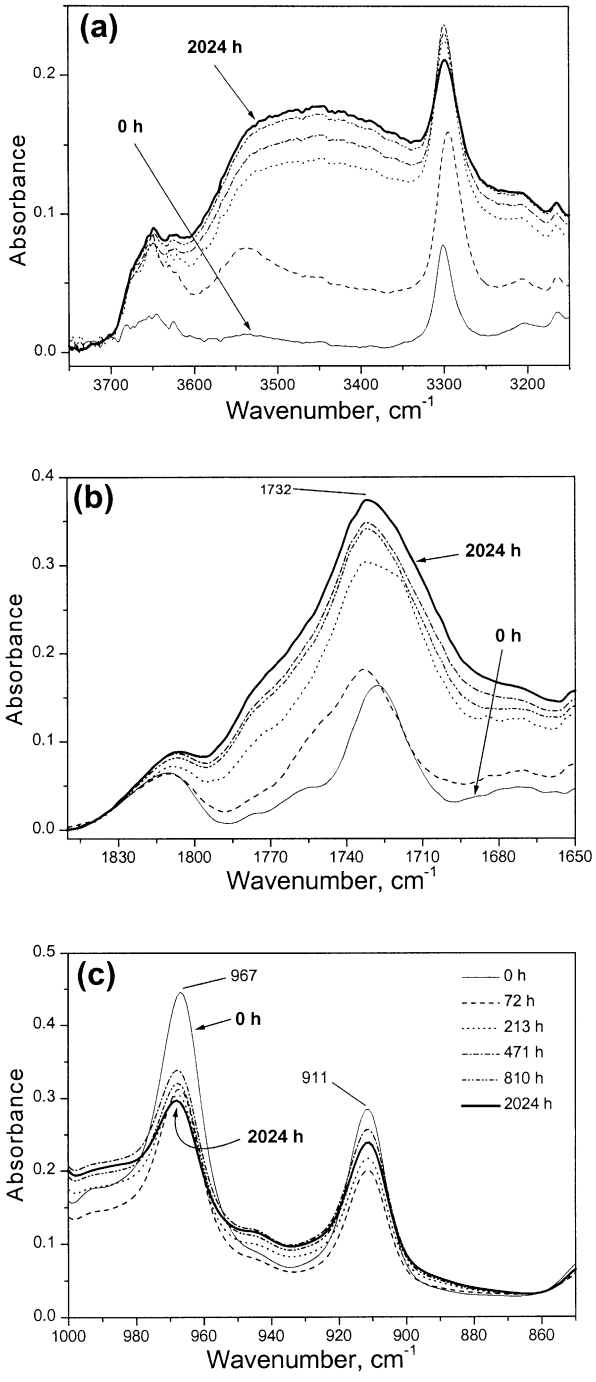

Fig. 7. ATR-FTIR spectra of section 1 (150 μm) as a function of irradiation time. a, hydroxyl region; b, carbonyl region: c, butadiene region.

times. Unmistakably, the degradation of ABS seems to be a direct result of the modification of the chemical structure of 1,4 PB, and not of 1,2 PB.

The time dependence of the hydroxyl absorbance, Fig. 8, shows an initial accelerated increase in the first 250 h of irradiation, and a moderate increase above 500 h of irradiation. The two regions were fitted well by straight lines, whose slopes are proportional to the rate of hydroxyl formation. The rates are 0.195 and 0.0034 h^{-1}, with correlation factors of 0.9984 and 0.833, respectively. The large difference between the two rates indicates that the formation of hydroxyls is a facile reaction that occurs in the initial stages of irradiation. The decrease of the hydroxyl intensity in the second stage is assigned to the hydroxyl consumption in degradation reactions, and/or to the decrease of the intensity from 1,4 PB as the degradation advances. Inset c in Fig. 5 clearly shows that the signal from 1,4 PB is not merely decreasing, but practically disappearing after 810 h of treatment.

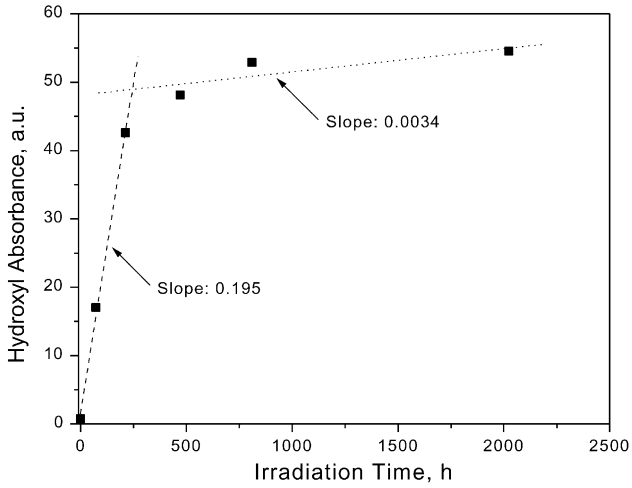

Fig. 8. Variation of the hydroxyl absorbance as a function of irradiation time. The linear fits for the initial and final portions of the plot have slopes of 0.193 and 0.0034 h^{-1}, respectively.

3.4. Comparison with previous studies on ABS degradation

The data described earlier suggest that the degradation of ABS upon UVB irradiation differs from the degradation due to radiation with $\lambda > 300$ nm [14,15] in two important ways. The first major difference is in the behavior of the two absorptions from butadiene: The results presented above indicate that 1,4 PB is attacked preferentially compared to 1,2 PB. In contrast, a major conclusion included in Refs. [14,15], is that the intensity of both components decreases rapidly. The degradation mechanism proposed for irradiation with $\lambda > 300$ nm [14,15] is based on the attack of an allyl proton adjacent to the double bond in butadiene; as this proton exists in both 1,4 and 1,2 butadiene units, we must conclude that the degradation mechanism for UVB and $\lambda > 300$ nm irradiation are significantly different. We note that our conclusions differ from those in Ref. [15] also in the behavior of the styrene component. For UVB treatment, our results showed no measurable change in the aromatic C–H stretches or in the peaks from the aromatic ring, when normalized by the C≡N stretch of the AN component; we note however, that the conclusion that the behavior of the styrene component in ABS and in polystyrene are similar is based on UV studies [15], not on the IR spectra.

The results presented in this study also differ when compared with conclusions deduced from irradiation of ABS by a Xe-arc [16]; that study concluded that the AN and B components are degraded, in contrast to the present study, which showed that the intensity of the AN component is stable. Clearly, the degradation mechanism in ABS is sensitive to the wavelength of the irradiation source.

4. Conclusions

The spatial variation of the degradation process in ABS exposed to UVB radiation ($\lambda = 290$–330 nm) and oxygen was studied by ATR-FTIR. The polymer contained 2 wt% Tinuvin 770, a HAS. The irradiation was performed in a weathering chamber at 318 K. ABS samples of thickness 4 mm were microtomed, and sections of thickness 50 and 150 μm were studied. For irradiation times up to ≈2000 h, the spectra indicated that the degradation of ABS by UVB irradiation is due to the disappearance of the double bonds in the 967 cm^{-1} peak from the 1,4 butadiene units; and that the SAN matrix is not altered.

The degradation is spatially heterogeneous; ATR-FTIR profiling indicated that the major effects due to the UVB irradiation occur in a layer of thickness ≈50 μm. In the directly irradiated layer, major damage was reflected in the appearance of the hydroxyl (3600–3200 cm^{-1}) and the carbonyl (1800–1600 cm^{-1}) peaks, and the disappearance of the butadiene peak at 967 cm^{-1}. The peaks representing the butadiene component were also affected by thermal degradation, which was detected on the nonexposed side of the sample, but not in the middle of the sample.

The present study confirmed and complemented the 1D and 2D nondestructive ESRI study performed on the same samples in our laboratory, which was based on the nitroxide radicals derived from the HAS [18–21].

Acknowledgements

This study was supported by the Polymers Program of the National Science Foundation. We thank Dow and Ciba Companies for the gift of ABS and HAS, respectively. Special thanks are due to M.V. Motyakin for his help with sample preparation and treatment, and for numerous helpful discussions; and to G. Grabowski, Department of Biology, University of Detroit Mercy, for his help with the instrumentation and practice of microtoming. The authors are grateful to the reviewers for their careful reading of the manuscript and constructive criticism.

References

[1] Product Focus: ABS, http://www.chemweek.com/marketplace/product_focus/2000/ABS. html (accessed 14 May 2001).
[2] Tullo AH. Chem Engng News 2001;79:15.
[3] Kulich DM, Pace JE, Fritch Jr LW, Brisimitzakis A. In: Kroschkowitz J, editor. 4th ed. Kirk–Othmer encyclopedia of chemical technology, vol. 1. New York: Wiley, 1991. p. 391.
[4] Aoki Y, Hatano A, Tanaka T, Watanabe H. Macromolecules 2001;34:3100.
[5] Steeman PAM, Meier RJ, Simon A, Gast J. Polymer 1997;38:5455.
[6] Kulich DM, Gaggar SK. In: Clough RG, Billingham NC, Gillen KT, editors. Polymer durability: degradation, stabilization and lifetime prediction, Advanced Chemistry Series 249. Washington: American Chemical Society, 1996. Chapter 31, p. 483.
[7] Hill DJT, Le TT, O'Donnell JH, Perera MCS, Pomery PJ. In: Reichmanis E, Frank CW, O'Donnell JH, editors. Irradiation of polymeric materials: processes, mechanisms, and applications. Washington: American Chemical Society, 1993.
[8] O'Donnell JH. In: Reichmanis E, O'Donnell JH, editors. The effects of radiation on high-technology polymers. Washington: American Chemical Society, 1989. Chapter 1, p. 1–13.
[9] Clough RG, Billingham NC, Gillen KT, editors. Polymer durability: degradation, stabilization and lifetime prediction Advanced Chemistry Series 249. Washington: American Chemical Society, 1996.
[10] Scott G. Macromolecular and polymer-bound antioxidants. In: Scott G, editor. Atmospheric oxidation and antioxidants, vol. II. Amsterdam: Elsevier, 1993. Chapter 5, p. 279–326.
[11] Gerlock JL, Kucherov AV, Smith CA. Polym Degrad Stab 2001;73:201 and references therein.
[12] Mailhot B, Gardette JL. Macromolecules 1992;25:4127 and references therein.
[13] Mailhot B, Jarroux N, Gardette JL. Polym Degrad Stab 2000;68:321.
[14] Jouan X, Gardette JL. J Polym Sci A 1991;29:685.
[15] Jouan X, Gardette JL. Polym Degrad Stab 1992;36:91.
[16] Carter III RO, McCallum JB. Polym Degrad Stab 1994;45:1.
[17] Celina M, Wise J, Ottesen DK, Gillen KT, Clough RL. Polym Degrad Stab 1998;60:493.
[18] Motyakin MV, Gerlock JL, Schlick S. Macromolecules 1999;32:5463.
[19] Kruczala K, Motyakin MV, Schlick S. J Phys Chem B 2000;104:3387.
[20] Motyakin MV, Schlick S. Macromolecules 2001;34:2854.
[21] Urban MW. Attenuated total reflectance spectroscopy of polymers: theory and practice. Washington: ACS, 1996.
[22] Koenig JL. Spectroscopy of polymers. 2nd ed. New York: Elsevier, 1999.
[23] Schlick S, Bokria JG. Polym Prepr (Am Chem Soc Div Polym Chem) 2001;42:244.
[24] Lin-Vien D, Colthup NB, Fateley WG, Grasselli JG. The handbook of infrared and Raman characteristic frequencies of organic molecules. New York: Academic Press, 1991. p. 143.
[25] Smith B. Infrared spectral interpretation: a systematic approach. New York: CRC Press, 1999.
[26] Howe DV, Wolkowicz MD. Polym Engng Sci 1987;27:1582.
[27] Aoki Y, Watanabe M. Polym Engng Sci 1992;32:878.